Airfoil Tip Vortex Formation Noise

Thomas F. Brooks* and Michael A. Marcolini*
NASA Langley Research Center, Hampton, Virginia

Spectral data are presented for the noise produced due to turbulent three-dimensional vortex flow existing near the rounded tip of lifting airfoils. The results are obtained by the comparison of sets of two- and three-dimensional test data for different airfoil model sizes, angles of attack, and tunnel flow velocities. Microphone cross-correlation and cross-spectral methods are used to determine the radiated noise. Corrections are made for tunnel shear-layer and source directivity effects. Interpretation of the results is aided by a three-dimensional flow analysis developed for this study which determines open wind tunnel and finite aspect ratio corrections heretofore neglected in tip vortex studies. Hot-wire measurements are made in the tip vortex formation region for the specification of governing flow parameters. The spectral data are normalized in a format considered most useful for quantitative prediction of this noise mechanism for practical systems such as helicopter rotors. A recommended prediction method is given.

Introduction

TIP vortex formation noise is a rotor blade self-noise mechanism known to contribute to rotor high-frequency broadband noise.[1,2] The importance of the tip region was first suggested by Lowson et al.[3] based on tests on a low-speed fan, where tip shape changes influenced the high-frequency broadband noise. More recent studies of the tip region involved noise measurements of stationary three-dimensional airfoil sections in wind tunnels. Kendall[4] used a directional microphone system to observe that noise sources are concentrated at the tips of wings and flaps. Fink and Bailey,[5] also using a directional microphone system, compared the source intensities for trailing-edge noise along the midspan and tip region of an airfoil model. For moderate angles of attack the source intensities were 5-10 dB higher near the tip. At higher angles, where stall occurred, the evidence of tip noise disappeared giving way to low-frequency separated flow noise, which was approximately uniform over the span. The absence of tip noise was apparently due to the loss of the tip vortex strength associated with the stalled condition. While these experimental studies did not produce the type of quantitative data required to formulate prediction models, they provided a better understanding of the noise mechanism.

George et al.[6] were the first to articulate a physical model of the tip noise mechanism. The noise was identified with the turbulence in the local separated flow region associated with the formation of the tip vortex. The flow is illustrated in Fig. 1 for an airfoil at angle of attack α to the flow of velocity U. The flow over the blade tip consists of a vortex of strength Γ with a thick viscous core. The recirculating flow within the core is highly turbulent. The mechanism for noise production is taken as trailing-edge noise due to the passage of this turbulence over the trailing-edge portion of the tip region. George et al.[6] used the trailing-edge noise analysis of Amiet[7] and Schlinker and Amiet[8] to obtain predictions after approximations were made of the surface pressure spectra, vortex velocity values, and the size (ℓ in Fig. 1) of the separated flow region at the tip. Subsequently, George and Chou[2] modified the original analysis by recommending a different pressure spectral model. However, there has been no experimental confirmation of the tip noise prediction modeling.

The purpose of this study is to isolate tip vortex noise, for the first time, in a quantitative manner and to propose a prediction method. The data are obtained by comparison of sets of two- and three-dimensional test results for different airfoil model sizes, angles of attack, and tunnel flow velocities. Stationary model results such as these should apply directly to helicopter rotor blades, as long as the loading characteristics are properly accounted for near the tips. The three-dimensional models used in the tests have rectangular planforms with rounded tips. The premise of the comparison method is that the three-dimensional (3D) models produce both tip vortex and turbulent boundary-layer/trailing-edge (TBL/TE) noise, while the two-dimensional (2D) models produce only the latter. While the data processing is extensive, utilizing microphone cross-correlation and cross-spectral methods, the result for each test case is a single spectrum that is corrected for shear-layer refraction and source directivity effects. The use of the spectral data in the examination of scaling laws is aided by a three-dimensional flow analysis to account for open wind tunnel and finite aspect ratio effects on the tip region aerodynamic loading. Hot-wire measurements in the tip region permitted the specification of flow parameters required by the scaling laws. The end result is a quantitative prediction capability for rounded tip blades, in general agreement with the approach of George et al.[6]

Experiment

The data in this report come from a comprehensive broadband noise experiment that consists of both noise and turbulence measurements for stationary airfoil section models in a wind tunnel. In order to study the tip vortex noise, models were tested using both two- and three-dimensional configurations. Testing parameters included model chord length, flow velocity, angle of attack to the flow, and boundary-layer transition through either natural transition or tripping. The details of the measurements and the facility have been reported previously.[9] Specific information applicable to this paper will be described here.

Models and Instrumentation

The models were tested in the low-turbulence potential core of a free jet located in an anechoic chamber. The jet was pro-

Presented as Paper 84-2308 at the AIAA/NASA Ninth Aeroacoustics Conference, Williamsburg, VA, Oct. 15-17, 1984; received Nov. 5, 1984; revision received May 28, 1985.

*Aerospace Technologist, Aeroacoustics Branch, Acoustics Division.

vided by a rectangular nozzle with exit dimensions of 30.48 × 45.72 cm. The chord lengths of the models range from 5.08 to 30.48 cm. The span of the 2D configuration models is 45.72 cm, while the 3D configuration models, shown in Fig. 2, all have spans of 30.48 cm. The trailing edge of each model is razor sharp, and the 3D models have rounded tips. The rounded tip was defined by rotating the NACA 0012 shape about the chord line at 30.48-cm span. Boundary-layer tripping was accomplished using a dense but nonoverlapping distribution of grit with a nominal particle "diameter" of 0.29 mm. This grit was attached to the model's surface from the leading edge to 20% chord. This heavy grit distribution ensured a fully developed turbulent boundary layer for even the smallest models. The two-dimensional flow conditions were provided by flush mounting the 2D models between two sideplates, each 152 × 30 × 1 cm, which were themselves flush-mounted to the nozzle lips. The 3D models were mounted to one sideplate, with the other sideplate removed. Acoustic data were obtained using an array of microphones, shown in Fig. 3 with the 3D test configuration. The data given herein were obtained from microphones 4 and 5, which were chosen because they provided an acceptable tradeoff between signal-to-noise ratio and source directivity. The signals were recorded on an FM tape recorder operated to provide a flat frequency response to 40 kHz. Turbulence measurements were made using miniature (0.5-mm spatial resolution) cross-wire probes in the near wake. The probe's orientation was such that the "u'" velocity component corresponded to the model chordline direction. The probe, as shown in Fig. 4 near the tip of a 3D model, was positioned using a three-axis computer-controlled traverse. Turbulence measurements near the tip of this model will be shown here. Acoustic data are presented for flow velocities of 71.3 and 39.6 m/s, with geometric angles of attack α_i in the tunnel of 0, 5.4, 10.8, and 14.4 deg.

Tip Vortex Measurement

Flow measurements were made across the span and near the tip of the 15.24-cm-chord 3D model to examine the boundary layer and the tip vortex formation. See Fig. 4. The probe traverses were made perpendicular to the chord line 1.3 mm behind the trailing edge at a number of locations along the span. The strong rotational gradients and finite resolution of the cross-wire probes combine to make the measurements subject to interpretation error. Similar concerns were found by Francis and Kennedy[10] in their efforts to reconstruct a tip flowfield using cross-wire data. No corrections are attempted here. It is believed, however, that the uncorrected u' velocity component data were accurate to within 10% for each measurement location. This should be sufficient for the present purposes of determining approximate tip vortex formation region dimensions and velocity scaling with angle of attack.

The turbulence intensity measurements u' from the traverses are input to a contour plotting program which interpolates between the discrete traverse locations and draws smoothed contours of equal intensity. Figure 5 shows these contours in the tip region on the suction side of the model at four different angles of attack. These contours are plotted at 1% intervals beginning at 1% intensity. The ordinate $y - s/2$ is zero at the tip, with $s/2$ representing the actual model span. The actual measurement locations along the span are indicated on the figure. For the zero angle-of-attack case shown in Fig. 5a, a fairly uniform boundary-layer flow is found over the span and tip. Nonuniformity seen may represent measurement error. As the model angle of attack is increased in Figs. 5b and 5c, a region of increasing intensity and size forms near the tip of the model, which indicates the formation of the tip vortex. In Fig. 5d, the rollup region has grown even larger, with corresponding increases in the intensity levels. The figures show that within the rollup formation region there are several localized pockets of turbulent activity around an apparent central core. As α is increased, the boundary layer slightly inboard of the tip becomes more compressed due to the severe downwash and crossflow in that region. The boundary layers away from the tip region were found to be very similar to the corresponding 2D configuration cases as documented in Refs. 9 and 11. With regard to mean flow conditions in the tip region, measurements indicated that the maximum velocities U_m corresponded roughly to the regions in and about that of maximum turbulence intensities. The values of U_m/U were approximately 0.9, 1.0, 1.2-1.3, and 1.3-1.45 for the 0-, 5.4-, 10.8-, and 14.4-deg cases, respectively.

Acoustic Spectral Determination

An overall self-noise spectrum contains tip vortex noise and turbulent boundary-layer/trailing-edge (TBL/TE) noise as well as any contaminants, such as that due to the sideplate's turbulent boundary layer impinging on the leading edge.[9] The TBL/TE noise is modeled as a source of dipole character located along the entire span of the trailing edge. The 2D

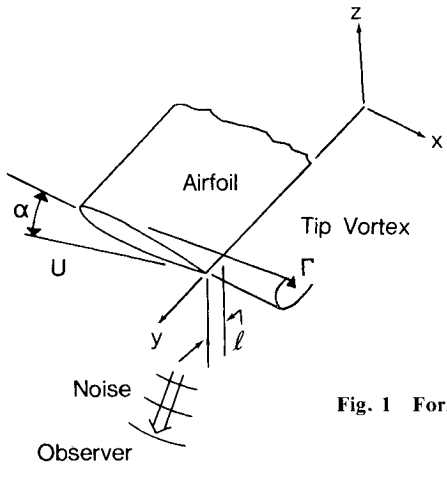

Fig. 1 Formation of tip vortex.

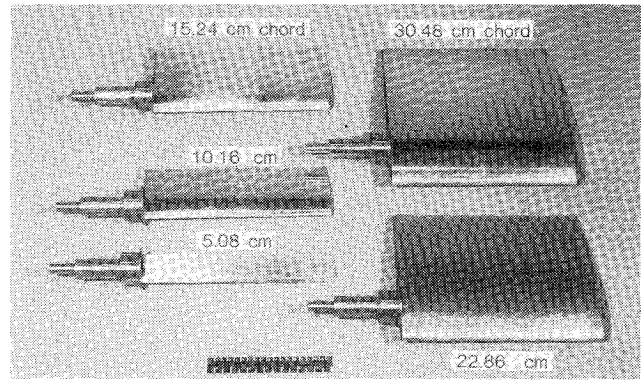

Fig. 2 NACA 0012 wing test models (3D configuration).

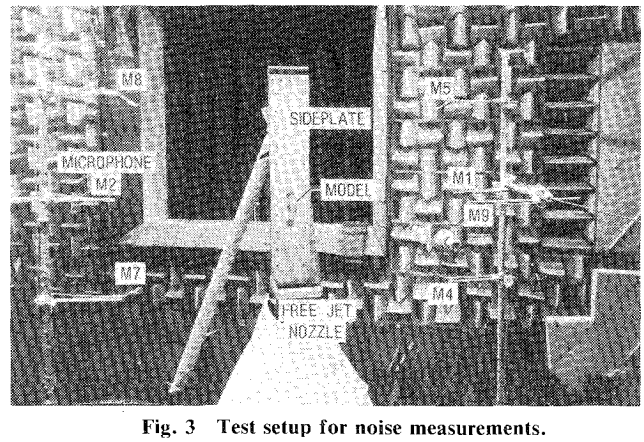

Fig. 3 Test setup for noise measurements.

models should produce only TBL/TE noise, while the 3D models should produce TBL/TE noise over most of the span with tip vortex noise radiating from the tip region of the trailing edge. Hence, the tip noise is obtained by the difference between the 3D and 2D model spectra for a given case, with 2D model spectrum scaled down to account for its longer span, which produces more TBL/TE noise. This approach assumes a balance between and linear superposition of noise mechanisms. Note that the turbulent intensity measurements of Fig. 5, for $\alpha > 0$, show clear distinction between boundary-layer and tip flow regions. The separation of noise mechanisms is further supported by a subsequent aerodynamic loads analysis.

Model Spectra

Each 2D and 3D model spectrum is obtained using a multistep process which accounts for the background noise, i.e., the noise produced by the particular test hardware with no model in the test setup. First, the cross correlation between microphones 4 and 5 is obtained using a Spectral Dynamics SD-360 FFT analyzer with 4096 averages. Then the cross correlation of the background noise for these microphones is subtracted to remove contaminants such as noise from the nozzle lip, as illustrated in Ref. 9. It has been shown that, at the delay time corresponding to the trailing-edge location, the cross correlation should represent the autocorrelation of the trailing-edge noise. This correlation is then transformed into the frequency domain via a Fourier transform which renders a cross spectrum with amplitude representing the power spectral density (PSD) of the sound field due to trailing-edge emission. For each microphone, corrections are calculated for shear-layer refraction, using Amiet's approach,[13] and trailing-edge noise directivity.[12] These corrections yield a spectrum that is corrected to effective sound field observer locations normal to the chord line at the trailing edge of the model. Each spectrum is then summed into a one-third octave spectrum where phase is neglected to avoid a negative bias in the pressure-squared summing.

Typical spectra produced by this technique are given in Fig. 6 for 2D and 3D cases at zero angle of attack for the 15.24-cm model. With no tip vortex noise present in this no-lift case, the only self-noise source present should be TBL/TE noise. With model and flow conditions matched here, the spectra should differ only by an amount due to differences in span length L. Based on a 10 log (L) dependency, a 1.8-dB difference between the two spectra is expected, which seems to agree with these results over most of the frequency bands. The extent of disagreement is due to 2D and 3D test rig effects not fully accounted for in the background corrections. However, the data seem to imply that these effects are small.

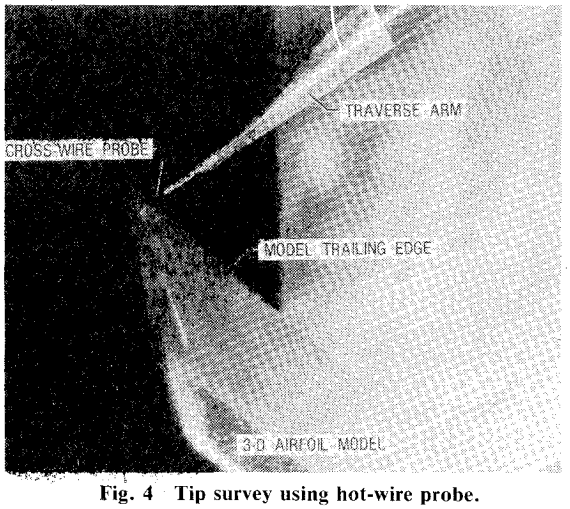

Fig. 4 Tip survey using hot-wire probe.

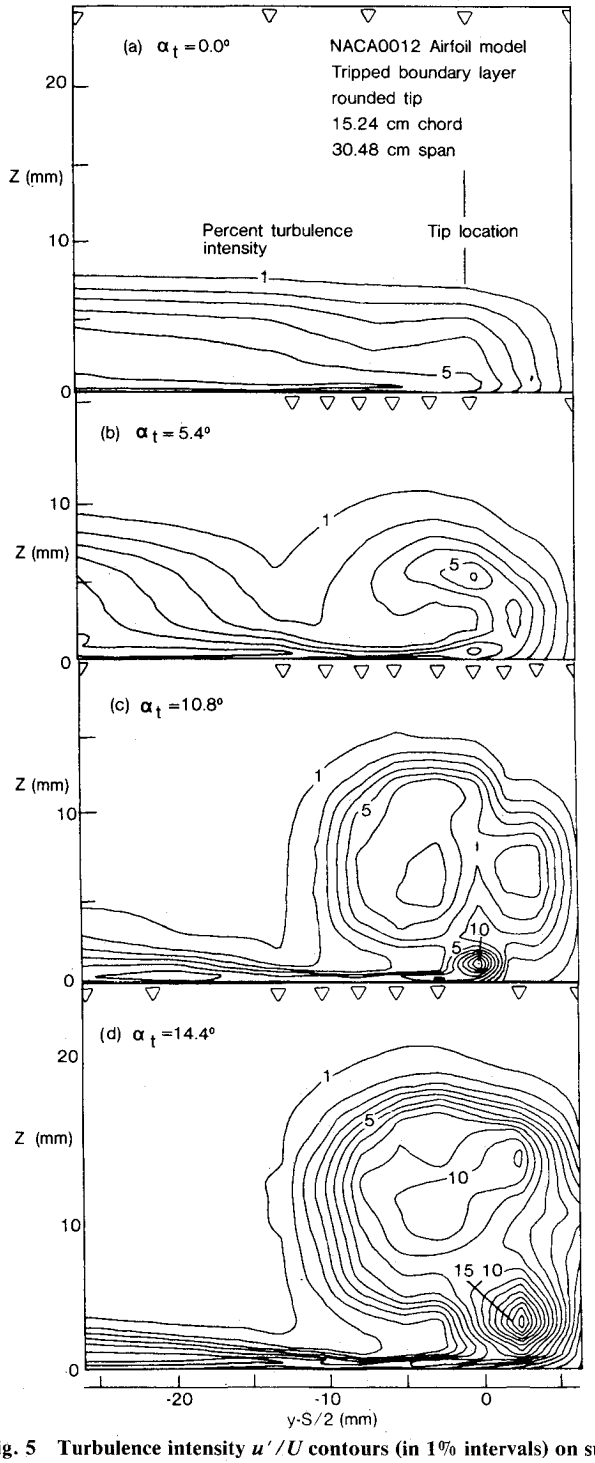

Fig. 5 Turbulence intensity u'/U contours (in 1% intervals) on suction side of tip region for different tunnel angles α_t. The tunnel velocity is $U = 39.6$ m/s. The symbols ▽ at top of figures indicate y measurement locations.

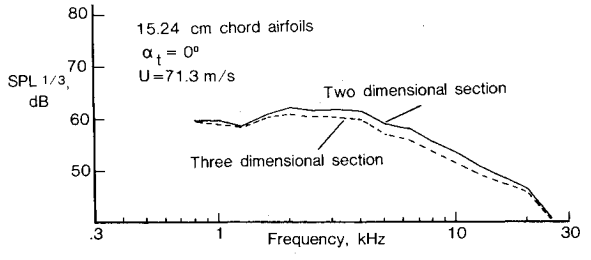

Fig. 6 One-third octave spectra for corresponding 2D and 3D cases at zero angle of attack.

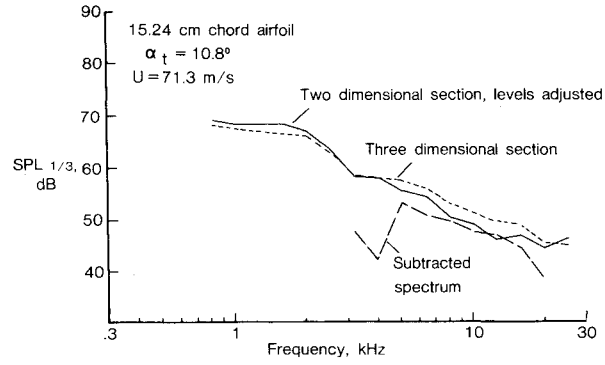

Fig. 7 One-third octave spectra for a 3D, and adjusted 2D, an resultant tip noise spectra for model at tunnel angle of $\alpha_t = 10.8$ deg.

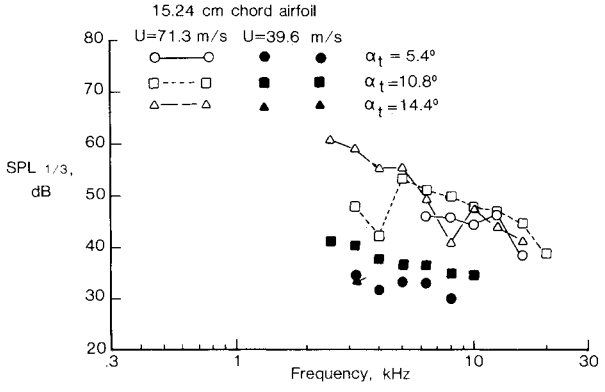

Fig. 8 Tip vortex noise, one-third octave spectra for the 15.24-cm case for two velocities and three tunnel angles.

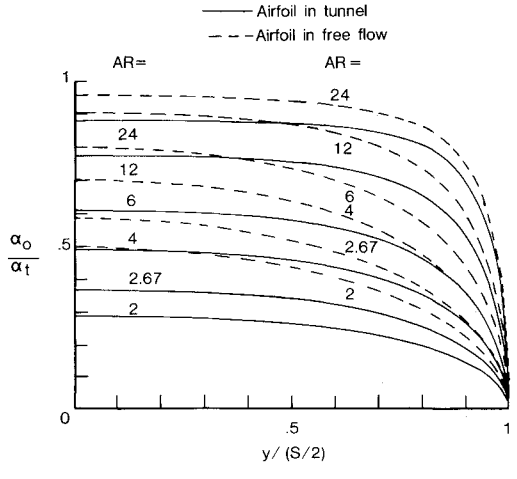

Fig. 9 Ratio of effective angles of attack to tunnel angles as a function of span for different aspect ratio wings for both tunnel and free-flow cases.

Tip Noise Spectra

Figure 7 shows spectra for the 15.24-cm-chord models as in Fig. 6, but now the angle α_t is 10.8 deg. The 3D test is as given, but the 2D result has been adjusted down in level to account for span difference and test rig effects discussed previously. The adjustments are the subtracted one-third octave levels in decibels between the curves of Fig. 6. The differences, now on a pressure-squared basis, between the 3D test result and the adjusted 2D results should represent the tip noise contribution to the 3D test condition. It is assumed here that contributions from any contaminants, such as leading-edge noise, substantially cancel in the subtraction process.

The results of this process for the 15.24-cm-chord tripped data at three angles for each of two speeds are shown in Fig. 8. Data are presented where the subtraction process rendered positive pressure levels. The subtraction process is very sensitive to errors in the individual spectra, due to the small differences between them. For example, in a particular one-third octave band, if two spectra to be subtracted were ideally only 1 dB apart, a +1-dB error in one spectrum would produce an error from +3.5 to $-\infty$ dB in that band for the tip noise spectrum. With this error amplification problem, substantial scatter may be expected in the tip noise data. This scatter is evident in Fig. 8. Where one might expect smooth spectral shapes, the scatter apparently masks any such shape. The greatest confidence is in the midrange for each spectrum where the tip noise had the highest relative levels compared to that of TBL/TE noise.

Acoustic Modeling

The analysis starts with results from trailing-edge noise theory. Consider the case of turbulence convecting at constant low-subsonic velocity U_c above one side of a large rigid plate. The turbulence remains spatially homogeneous as it passes over the edge and away from the plate. The far-field observer is at a distance R on a line perpendicular to the plate at the trailing edge. The predicted sound field spectrum $S(f)$ is

$$S(f) \simeq \frac{1}{8\pi^2 R^2}\left(\frac{U_c L}{c_0}\right)\ell_y(f)\Phi(f) \tag{1}$$

where L is the spanwise (y coordinate) extent of the edge "wetted" by the turbulent flow, c_0 the speed of sound, and $\Phi(f)$ the power spectral density of the surface pressure far enough upstream[12] so that edge pressure scatter (noise) is unimportant. The term $\ell_y(f)$ is the lateral integral scale of the unsteady surface pressure. If the coherence of the pressure field falls off exponentially,[12,8] $\exp[-\zeta 2\pi f|\Delta y|/U_c]$ for sensors separated by distance Δy, then $\ell_y(f) = U_c/\zeta 2\pi f$, where ζ is an empirical constant.

George et al.[6] used a trailing-edge noise result consistent with Eq. (1), but generalized it for a rotating blade configuration. The "wetted" distance "L" was identified with the spanwise extent "ℓ" at the trailing edge of the separation due to the tip vortex. This, as well as velocity values, was estimated based on flowfield documentation of Shivananda et al.[14] for blade tips. To obtain $\Phi(f)$, a simplified cross-flow analogy was employed to justify the use of surface pressure data from the 2D flow correlation studies of Mabey[15] and Fricke.[16] In a later version of the analysis, George and Chou[2] use surface pressure data from delta wing studies of Richards and Fahy[17] and Peckham[18] to replace the normalized 2D data. Also remodeled were length and velocity scales for both rounded and flat tips. These were based on an extrapolation of measured data from the tip vortex flow studies of Gray et al.[19] and Chigier and Corsiglia.[20] The form taken for surface pressure is

$$\Phi(f) = \Phi(\hat{f})\ell q^2/U_m$$

where $q = 0.5\rho U_m^2$; ρ is the medium density, $\hat{f}$ the normalized frequency $f\ell/U_m$, and U_m the maximum velocity along the separation streamline. The length ℓ and velocity U_m are functions of the local tip angle of attack α. The analysis ignores the fact that the flow near the tip is skewed and the surface pressure statistics are spanwise inhomogeneous. The spectrum is assumed to be constant over the distance ℓ.

If one adapts the scaling premise from above, Eq. (1) can be used as a basis for normalization of the acoustic spectra measured in the present study. Equation (1) becomes, for scaled one-third octave band sound pressure level, "scaled"

$SPL_{1/3}$ in units of dB:

$$SPL_{1/3} - 10\log\left[\frac{M^2 M_m^3 \ell^2}{R^2}\right] = 10\log\left[\frac{0.2308 c_0^4 (\rho/g)^2}{64\pi^3 \zeta p_0^2}\left(\frac{M_c}{M}\right)^2\right] + 10\log\Phi(\hat{f}) \qquad (2)$$

where M, M_c, and M_m are the Mach numbers corresponding to U, U_c, and U_m. The arrangement of Eq. (2) is advantageous because the undetermined parameters requiring the crudest approximations, i.e., ζ, M_c, and $\Phi(\hat{f})$, are grouped to the right-hand side (RHS). The left-hand side (LHS) is subsequently used to normalize measured data. The dependence of M_m and ℓ on angle of attack α is evaluated after the following aerodynamic analysis.

Aerodynamic Analysis

The model angles of attack, α_t, are reinterpreted here to account for the tunnel and finite aspect ratio effects on the aerodynamics of the inboard and tip regions.

The testing of airfoil models in the finite-sized open wind tunnel causes flow curvature and downwash deflection of the incident flow that do not occur in free air. Brooks et al.[11] use lifting surface theory to develop the 2D open wind tunnel corrections to angle of attack and camber. Upon ignoring small camber effects, of interest here is an effective angle of attack α_* representing the angle in free air required to give the same lift as α_t would give in the tunnel. For the present 2D configuration, α_*/α_t equals 0.88, 0.78, 0.62, 0.50, 0.38, and 0.30 for the 2.54-, 5.08-, 10.16-, 15.24-, 22.86-, and 30.48-cm-chord models, respectively. For the present problem, these results require comparison with that obtained for the 3D configuration.

The 3D open wind tunnel correction problem is treated in Ref. 21. Key results are given here for sectional characteristics for different model spanwise positions y. The lift per unit span is

$$L'(y) = \rho U \Gamma(y) \qquad (3)$$

where $\Gamma(y)$ is the local vortex strength. One can define an effective angle of attack $\alpha_0(y)$ to satisfy

$$\alpha_0(y) = \Gamma(y)/\pi U c \qquad (4)$$

where c is the chord length. Curves of $\alpha_0(y)/\alpha_t$ vs y normalized by the half-span (full experimental model span) $s/2$ are given in Fig. 9. Note that this is called half-span because the tunnel models are mounted to a hard-wall sideplate giving a mirror image of itself for the wind tunnel analysis approach, thereby doubling the effective span. For convenience, the curves in Fig. 10 are labeled by the respective aspect ratios, $\mathcal{R} = s/c = 24$ and 12 for the 2.54- and 5.08-cm-chord airfoil, etc. There are two curves given for each $\mathcal{R}$—one corresponding to the experimental tunnel conditions and the other to what would occur in free unbounded flow for the same aspect ratio wing. It is seen that the tunnel cases render uniformly less lift per unit span (less effective angle of attack) than for the same wing in free flow. Increasing $\mathcal{R}$ increases the loading. For the limiting case of $\mathcal{R} \to \infty$ for free flow $\alpha_0(y)/\alpha_t$ approaches the value of 1 for all $y/(s/2)$ values less than 1. For $\mathcal{R} \to \infty$ (by allowing $s \to \infty$) for the tunnel cases $\alpha_0(y)/\alpha_t$ approaches the values of α_*/α_t for the two-dimensional corrections. An important point to observe from Fig. 9 is that $\alpha_0(y=0)/\alpha_t$ already is approximately α_*/α_t for each of the tunnel $\mathcal{R}$ cases. This means that the two-dimensional test environment is approximately duplicated near the sideplate in a 3D test configuration.

With this established for the inboard region, it is now desired to define an effective tip angle α_{tip} for the models that

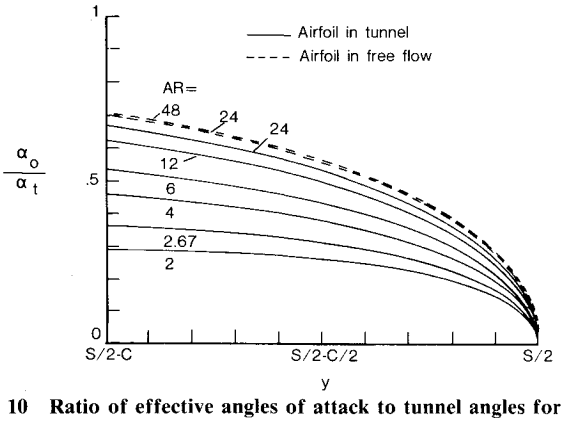

Fig. 10 Ratio of effective angles of attack to tunnel angles for different aspect ratio wings in the tip region.

incorporate the effects of tunnel and finite aspect ratios on the formation of the tip vortex. For a particular α_{tip}, c, and U, the same tip vortex is produced. This should allow the unique specification of U_m/U and ℓ/c in terms of α_{tip}. From inviscid analysis for finite span wings, one expects the tip vortex strength Γ_{tip} to be proportional to the sectional lift slope $\partial L'(y)/\partial y$ near the tip. Therefore, α_{tip} can be defined referenced to some specific tunnel (or free flow) and $\mathcal{R}$ case as follows:

$$\alpha_{tip} = \left[\left(\frac{\partial L'/\partial y}{\partial L'/\partial y_{,\,ref}}\right)_{y \to s/2}\right]\alpha_t = \left[\left(\frac{\alpha_0}{\alpha_{0,\,ref}}\right)_{y \to s/2}\right]\alpha_t \qquad (5)$$

Here the RHS is due to the linear relationships in Eqs. (3) and (4). Figure 10 shows the tip loading for a spanwise extent equal to that of the chord of the individual models. This puts the results on an equal geometric basis for the evaluation of Eq. (5). Included in Fig. 10 for free unbounded flow is an $\mathcal{R} = 48$ case along with that of $\mathcal{R} = 24$ of Fig. 9. The nearness of the lines to one another reflects the fact that the high aspect ratio cases approximate the limiting $\mathcal{R} \to \infty$ case for free flow in the tip region. Using this limiting case as the reference, one obtains[21] for the models $\alpha_{tip}/\alpha_t = 0.95$, 0.89, 0.79, 0.71, 0.62, and 0.54 for the $\mathcal{R} = 24$, 12, 6, 4, 2.67, and 2 cases, respectively.

Scaling Results and Discussion

In this section the scaling procedure suggested by Eq. (2) is examined for measured tip noise spectra. The parameters required are specified based on the tip flow measurements, as well as the aerodynamic analysis which is used to match tip loading conditions betweeen the models of different sizes.

The tip flow results of Fig. 5 do not lend support to the relationship for length ℓ suggested by George and Chou[2] for the rounded tip case, i.e., $\ell/c = 0.0074(\alpha - 2)$ with α taken here as α_{tip} in degrees. The results suggest a proportional relationship with angle, consistent with the dimensional grouping of Eq. (4) of the linear aerodynamic analysis. One obtains roughly

$$\ell/c \approx 0.008\alpha_{tip} \qquad (6)$$

if one chooses the 4-5% turbulent-intensity contours as guides to determine length. The choice appears to give a reasonable indication of the spanwise extent of the vortex separation region. The relationship[2] for velocity

$$M_m/M \approx (1 + 0.036\alpha_{tip}) \qquad (7)$$

appears, however, to be in rough agreement (within 5-10%) with maximum velocity measurements corresponding to the maximum u'/U values in the vortex core region with α_{tip} again in degrees.

With the parameters of the LHS of Eq. (2) specified, tip noise spectra are normalized in Fig. 11 for five chord sizes and three angles of attack for the tripped boundary-layer models. Two tunnel speeds are given for three of the chord sizes. For clarity the $U=71.3$-m/s cases are given by line and symbol data, whereas the $U=39.6$-m/s cases are by symbols only. The scatter observed for the data is due to the amplification of error one gets from the subtraction process as previously discussed for Figs. 7 and 8. Due to the error scatter, there are a few test cases where the subtraction process produced a positive contribution to the noise in only one or two one-third octave bands. These data are presented but are indicated by flags to show that they may not be statistically significant.

Despite the scatter, the normalization of the data appears to have a substantial degree of success. This is illustrated well by comparing Fig. 11c to the corresponding 15.24-cm-chord cases of Fig. 8. The normalization affects large changes in the relative positions of the spectra to bring them into agreement. There is somewhat less agreement for the other chord sizes. In addition to scatter, there appears to be a trend for bias error with the larger chords scaling to lower levels. It is noted in the normalization that, if the actual angle α_t is used instead of the tip equivalent angle α_{tip}, the bias error becomes severe thereby preventing a successful data collapse. It should also be mentioned that other normalization attempts, performed for purposes of completeness, show that the data scales very poorly when ℓ is replaced by boundary-layer thickness δ and $M^2M_m^3$ is replaced by M^5. This is additional evidence that the subtraction process which rendered the data successfully eliminated any major contribution from boundary-layer/trailing edge noise. The present agreement suggests the correctness of the tip noise normalization premise, the choice of ℓ and M_m, and the use of α_{tip}.

The results presented thus far are for tripped airfoil models. For the untripped models, where the surfaces are kept smooth and clean, the useful data base is limited because laminar boundary-layer/vortex shedding noise[9] occurs to some extent for all but the largest chord and highest speed case tested. The presence of this high-frequency quasi-tonal noise serves to introduce substantial error in the subtraction process used to extract the tip noise spectra. Figure 12 shows the extracted tip noise for the untripped 30.48-cm-chord case at $\alpha_t=5.4$ deg for $U=71.3$ m/s scaled in the manner of Fig. 11. In this particular case no vortex shedding effects are observed and the data scale close to that of the corresponding tripped case in Fig. 11e. However, decreasing the velocity to $U=39.6$ m/s produced evidence in the individual spectra of shedding which contaminates the extracted spectrum also shown in Fig. 12 for illustrative purposes.

A curve is fitted to the tip noise spectral data and is included in Figs. 11 and 12. The curve is defined by

$$\text{Scaled SPL}_{1/3} = 126 - 30.5(\log \hat{f} + 0.3)^2 \qquad (8)$$

which is a parabolic fit about a peak Strouhal number of $f=0.5$. The fit seems to represent a reasonable compromise between the data. Comparing some of the present results to scaling proposed by George and Chou,[2] one finds[21] that their analysis tends to overpredict levels and underpredict peak frequencies. The difference, of course, is traceable to choices of parametric inputs, such as ℓ/c as discussed, obtained without benefit of pertinent data. This should not detract from the basic correctness of the analysis.

For application in predictive programs for rounded-tip blades, Eq. (8) can be equated to the LHS of Eq. (2). The obtained spectrum would be for observers located on a line normal to the chordline at the trailing edge. In application, the directivity associated with trailing-edge noise can be applied. In the use of Eqs. (6) and (7) to define ℓ and U_m, α_{tip} is correctly regarded as the actual geometric angle of attack of the tip to the incoming flow for the reference case of large aspect

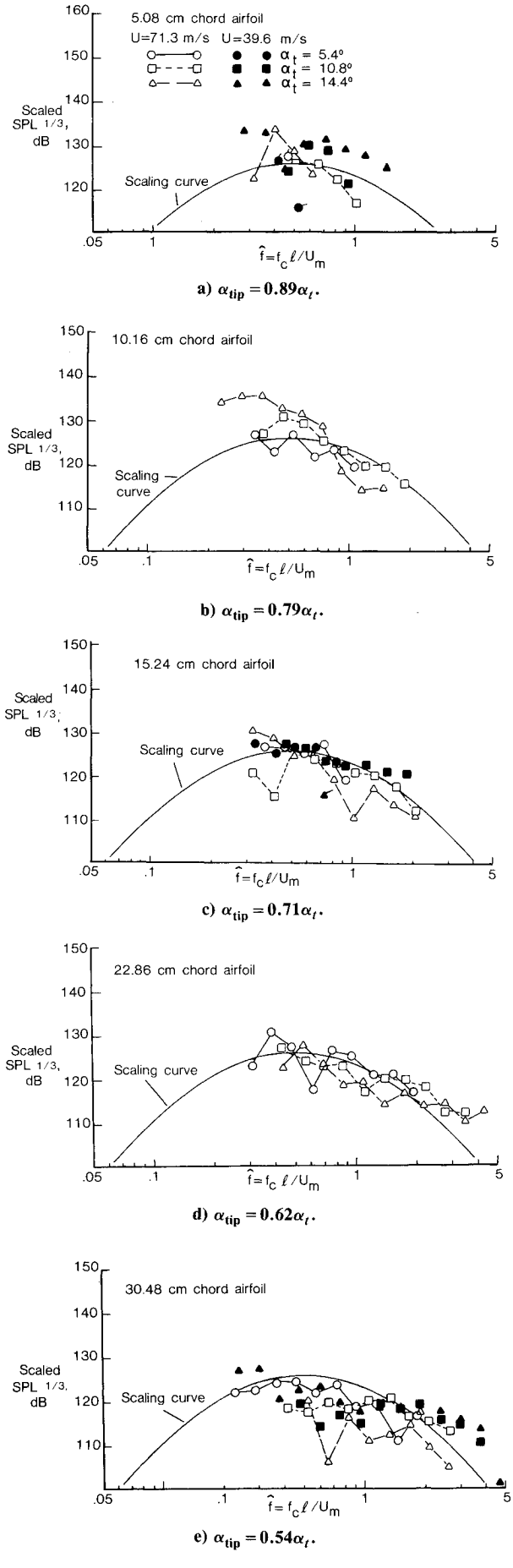

Fig. 11 Normalized tip noise spectra for five chords at different speeds and three angles of attack for tripped boundary-layer models. The fitted scaling curve is given by Eq. (8).

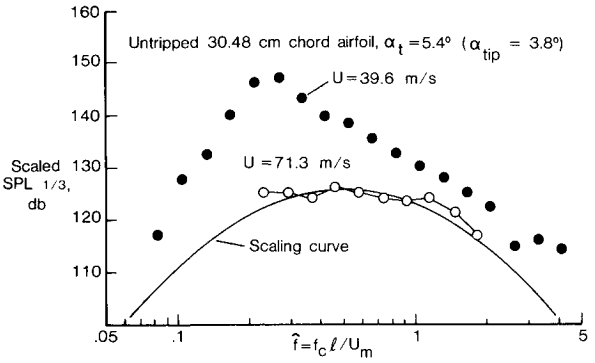

Fig. 12 Normalized tip noise spectra for the untripped boundary-layer 30.48-cm-chord model. The scaling curve is given by Eq. (8).

ratio wings with little or no twist near the tip. However, for cases where the tip loading characteristics may be different, such as for rotor and propeller blades, α_{tip} must be redefined based on computed sectional loading compared to the reference case ($\mathcal{R} = 48$ curve of Fig. 10) with the use of Eq. (5). For this application α_t in Eq. (5) is interpreted as the actual geometric angle to the oncoming flow. For cases where the tip loading is found to be high, this analysis will predict an increased importance of tip noise in comparison to boundary-layer/trailing-edge noise.

Conclusions

Tip vortex formation noise spectra for rectangular planform and rounded tips are determined for different airfoil model sizes, angles of attack, and tunnel flow velocities. Employing an aerodynamic analysis and the experimentally determined parametric inputs, a normalization of tip noise is achieved. This supports a scaling premise for the noise source first suggested by George et al.[6] A prediction method is proposed that should be applicable for twisted rotor and propeller blades as well as for wing tips. The method is applied to specific blade tips by a tip loads analysis.

For the stationary blade data shown, tip noise is of lesser importance to the overall broadband self-noise spectrum than boundary-layer/trailing-edge noise. This necessarily will not be so for rotor systems because of the tip's relatively higher velocities compared to the inboard regions of the blade and the tip loading which should be high. The tip noise should be included in overall spectrum prediction programs. For the cases where the tips are flat, one should expect a much more significant contribution to the noise field as indicated by calculations[2] employing flat tip flow modeling.

Acknowledgments

The authors would like to acknowledge the assistance of D.S. Pope of Kentron International for providing programming for the aerodynamic analysis.

References

[1] Brooks, T.F. and Schlinker, R.H., "Progress in Rotor Broadband Noise Research," *Vertica*, Vol. 7, No. 4, 1983, pp. 287-307.

[2] George, A.R. and Chou, S-T., "Broadband Rotor Noise Analysis," NASA CR-3797, April 1984.

[3] Lowson, M.V., Watmore, A.R., and Whitfield, C.E., "Source Mechanisms for Rotor Noise Prediction," NASA CR-2077, 1973.

[4] Kendall, J.M., "Measurements of Noise Produced by Flow Past Lifting Surfaces," AIAA Paper 78-239, 1978.

[5] Fink, M.R. and Bailey, D.A., "Airframe Noise Reduction Studies and Clean Airframe Noise Investigation," NASA CR-159311, April 1980.

[6] George, A.R., Najjar, F.E., and Kim, Y.N., "Noise Due to Tip Vortex Formation on Lifting Rotors," AIAA Paper 80-1010, June 1980.

[7] Amiet, R.K., "Noise Due to Turbulent Flow Past a Trailing Edge," *Journal of Sound and Vibration*, Vol. 47, 1976, pp. 387-393.

[8] Schlinker, R.H and Amiet, R.K., "Helicopter Rotor Trailing Edge Noise," AIAA Paper 81-2001, Oct. 1981; also, NASA CR-3470, Nov. 1981.

[9] Brooks, T.F. and Marcolini, M.A., "Scaling of Airfoil Self Noise Using Measured Flow Parameters," *AIAA Journal*, Vol. 23, Feb. 1985, pp. 207-213; also AIAA Paper 83-0785, April 1983.

[10] Francis, M.S. and Kennedy, D.A., "Formation of a Trailing Vortex," *Journal of Aircraft*, Vol. 16, March 1979, pp. 148-154.

[11] Brooks, T.F., Marcolini, M.A., and Pope, D.S., "Airfoil Trailing Edge Flow Measurements and Comparisons to Theory, Incorporating Open Wind Tunnel Corrections," AIAA Paper 84-2266, Oct. 1984.

[12] Brooks, T.F. and Hodgson, T.H., "Trailing Edge Noise Predictions Using Measured Surface Pressures," *Journal of Sound and Vibration*, Vol. 78, 1981, pp. 69-117.

[13] Schlinker, R.H. and Amiet, R.K., "Shear Layer Refraction and Scattering of Sound," AIAA Paper 80-0973, 1980.

[14] Shivanada, T.P., McMahon, H.M., and Gray, R.B., "Surface Pressure Measurements at the Tip of a Model Helicopter Rotor in Hover," *Journal of Aircraft*, Vol. 15, Aug. 1978, pp. 460-467.

[15] Mabey, D.G., "Analysis and Correlation of Data on Pressure Fluctuations in Separated Flow," *Journal of Aircraft*, Vol. 9, Sept. 1972, pp. 642-645.

[16] Fricke, F.R., "Pressure Fluctuations in Separated Flows," *Journal of Sound and Vibration*, Vol. 17, 1971, pp. 113-123.

[17] Richards, E.J. and Fahy, F.J., "Turbulent Boundary Layer Pressure Fluctuations over Two-Dimensional Surfaces and Narrow Delta Wings," *Acoustic Fatigue in Aerospace Structures*, Syracuse University Press, Syracuse, NY, 1965, pp. 39-62.

[18] Peckham, D.H., "Low-Speed Wind-Tunnel Tests on a Series of Uncambered Slender Pointed Wings with Sharp Edges," British ARC, R&M 3186, 1961.

[19] Gray, R.B., McMahon, H.M., Shenoy, K.R., and Hammer, M.L., "Surface Pressure Measurements at Two Tips of a Model Helicopter Rotor in Hover," NASA CR-3281, May 1980.

[20] Chigier, N.A. and Corsiglia, V.R., "Tip-Vortices—Velocity Distributions," NASA TMX-62087, 1971; also, Preprint 522, 27th Annual National V/STOL Forum of the American Helicopter Society, May 1971.

[21] Brooks, T.F. and Marcolini, M.A., "Airfoil Tip Vortex Formation Noise," AIAA Paper 84-2308, Oct. 1984.